Desalination and Water Treatment
www.deswater.com
doi: 10.5004/dwt.2019.24426

163 (2019) 297–309
September

Bisphenol S degradation using Fe-SBA-15/UV/US/peroxymonosulfate: performance optimization, biodegradability, mineralization and toxicity studies

Alireza Rahmani[a], Hadi Rahimzadeh[a,*], Mohammad-Taghi Samadi[a], Abbas Farmani[b], Ghorban Asgari[a]

[a]*Department of Environmental Health Engineering, Faculty of Health and Research Center for Health Sciences, Hamadan University of Medical Sciences, Hamadan, Iran, email: hadi_rahimzadeh@yahoo.com (H. Rahimzadeh)*
[b]*Dental Research Center, Hamadan University of Medical Sciences, Hamadan, Iran*

Received 12 February 2019; Accepted 15 May 2019

ABSTRACT

The presented research was to prepare the iron-doped SBA-15 catalyst (Fe-SBA-15) and to apply it as a heterogeneous catalyst in the ultrasound (US) and ultraviolet (UV) processes for developing the heterogeneous activation of peroxymonosulfate and degrading the bisphenol S (BPS). The effect of important reaction parameters on the removal of BPS by the Fe-SBA-15/UV/US/PMS process was investigated. Simultaneous use of US and UV irradiations with Fe-SBA-15 for activation of PMS led to significant degradation of BPS. The BPS degradation rate was developed at the presence of higher PMS and Fe-SBA-15 dosages at pH = 7. It was also found, based on the quenching tests, that both $OH^{\bullet}$ and $SO_4^{\bullet-}$ radicals have a superior role in the degradation of BPS and dominant species are the sulfate radicals. Complete removal of BPS and 67% mineralization degree was obtained at the optimum conditions after 60 min reaction. Based on the activated sludge inhibition assessment, it was detected that the toxicity of the solution significantly decreased in this system. Moreover, according to the BOD_5/COD ratio of samples, it was found that the biodegradability of treated samples is improved. Furthermore, it was confirmed that Fe-SBA-15 can be reused in five consecutive cycles and the removal efficiency was acceptable at 94.2%.

Keywords: Fe/SBA-15; Sulfate radical; Peroxymonosulfate; Sono-photo-oxidation; Bisphenol S

1. Introduction

Endocrine disrupting chemicals (EDCs) are of the chemicals which have the capability to interrupt the hormones in the body's endocrine system [1]. Nowadays, the concerns toward the EDCs have raised, due to widespread exposure of the communities to these material [2]. Epidemiologic evidence on the experimental animal suggested an association between the exposure to EDCs and the diseases such as fertility disorders, obesity, diabetes, cardiovascular disease, neurological disorders and reproductive disorders and development of types of cancer such as breast, ovarian, testicular and prostate [3,4]. EDCs include a wide range of compounds such as pharmaceuticals, pesticides, plasticizers and monomers, flame retardants, natural products, fragrances, industrial chemicals, surfactants, multi-ring aromatic compounds, chlorine compounds (PCBs, dioxins and furans) and food contact materials [4,5]. An important category of EDCs are the phenolic EDCs such as bisphenols (BPs), octylphenol (OP), nonylphenol (NP) and diethylstilbestrol (DES) [6]. After establishing the new rules and regulations to confine the production and use of the bisphenol A (BPA), due to the adverse effect associated, the production and consumption of bisphenol S (BPS), as an

* Corresponding author.

alternative to BPA, has been grown in many countries [7]. But, after a while, the detrimental and adverse effect of BPS on the life cycle has been identified and it has been introduced as a contaminant [8]. BPS or 4,4-sulfonyldiphenol has the chemical formula of $C_{12}H_{10}O_4S$ [7]. BPS is widely used as a monomer in the production of epoxy resins and glues. It has also been used as an important chemical additive in pesticides, dyestuffs, colorfast agents, leather tanning agents, dye dispersants and fiber improvers [9]. BPS is not biodegradable, and has the bioaccumulation property and can accumulate in the aquatic environment. Experiments have publicized that BPS is also a harmful EDC [10] and possesses the acute toxicity, genotoxicity and estrogenic activity, which it is comparable with BPA and can promote the lymphocyte proliferation in animals [11,12]. The application of conventional wastewater treatment does not always provide complete removal of all EDCs; hence, the effluent and sludge from WWTPs are significant sources for releasing these compounds into the environment [13].

Advanced oxidation processes (AOPs), which are based on the generation of extremely reactive species, for example, hydroxyl ($OH^{\bullet}$) and sulfate ($SO_4^{\bullet-}$) radicals, can be used to remove the resistant pollutants and even to reach the complete degradation when the conditions are optimal [14,15]. Sulfate radical-based AOPs using persulfate (PS, $S_2O_8^{2-}$) or peroxymonosulfate (PMS, HSO_5^-), as oxidant, have emerged as excellent methods for degradation of resistant contaminants [16]. Compared with hydroxyl radicals (E^0 = 1.8–2.7 V), SO_4^{2-} shows some advantages such as higher redox potential (E^0 = 2.5–3.1 V), longer half-life, stronger oxidation ability and higher degradation efficiency for most of the organic contaminant over a wide pH range (4 < pH < 9) [17,18]. The trade names of PMS are Caroat and Oxone. PMS is prepared through the reaction of H_2O_2 solution with oleum and an alkali potassium compound. PMS is a white crystalline solid, which is very stable, cheap, non-toxic, and easily soluble in water (>250 g L^{-1} at 20°C) [19]. PMS should be activated before use and there are several ways applied to activate the PMS which are including UV [20], US [21], thermal [22], heterogeneous catalysts [23], transition metal ions such as Fe^{2+}, Co^{2+} and Mn^{2+} [24,25], electrochemistry method [26]. For the efficient degradation of resistant contaminants, there is a need to increase the PMS decomposition rate through some ways. One way is the application of a combination of activation methods (hybrid systems). Some of these studies that used the hybrid methods for the activation of PMS are as follows: sonophotocatalytic process along with Fe-doped Bi_2O_3 and PMS for real textile wastewater remediation [27], UVC/PMS/Co_3O_4 for pulp and paper wastewater treatment [28], Co-TiO_2/UV/PMS for Rhodamine B (RhB) degradation [29], Fe^{2+}/UV/PMS for degradation of lindane [30], and Co^{2+}/US/PMS for degradation of amoxicillin [31]. Reviewing these papers reveals that the PMS decomposition rate and generation of sulfate radicals was considerably increased when hybrid methods were utilized and, finally, the maximum mineralization degree was achieved by the production of further sulfate radicals.

Therein, mesoporous SBA-15 is an excellent support, which has great specific surface areas, large pore diameters, ordered channel structure and higher thermal and hydrothermal stability [32]. Co^{2+} and ferrous ions are the most common transition metals as catalysts for the PMS activation. Because cobalt is toxic, even in very low concentrations, there are limitations to utilize this catalyst. In many studies, the iron nanoparticles have been used along with some carriers for activation of PMS [33]. Iron is a safe and low-cost element and is abundantly found in the earth's crust, and it is not a serious threat to human health and the environment; thus, its use for environmental application is justifiable and reasonable [33,34]. Moreover, Fe/SBA-15 is widely used in catalytic degradation of organic contaminants. For example, in the study of Jinisha et al. [35] for rhodamine B degradation, in the study of Sun et al. [36] for chromium (VI) removal and in the study of Shukla et al. [37] for phenolic contaminants oxidation.

The employment of US and UV with AOPs systems provides a better condition for generating further strong free radicals that enhance the degradation rate of pollutants. Decreasing the mass transfer limitations and providing a clean and reactive surface for catalyst are accounted for as the benefits of US, which these benefits have a direct and remarkable effect on the removal of the products from the catalyst surface [38]. In addition, the notable role of UV irradiation in the regeneration of Fe^{2+}, which enhances the production of extra strong free radicals and, subsequently, improving the degradation rate of contaminant, has been identified [38].

Hence, our goal in this study was the simultaneous application of three agents (Fe-SBA-15 as heterogeneous catalyst, UV and US) for activation of PMS and degradation of BPS. The BPS degradation efficiency by means of Fe-SBA-15/UV/US/PMS was assessed using key operational parameters including the solution pH, catalyst dosage, and PMS and BPS concentrations. The recyclability, durability, biodegradability, mineralization degree and toxicity assessment were also examined.

2. Experimental section

2.1. Chemicals

The following chemicals were used in this study:

Tetraethyl orthosilicate (TEOS, 98%), pluronic P123 ($EO_{20}PO_{70}EO_{20}$), iron(III) nitrate $Fe(NO_3)_3{\cdot}9H_2O$, BPS (≥98.0%) were purchased from Sigma-Aldrich Co., USA. Peroxymonosulfate, sodium hydroxide, ethanol, *t*-butanol, sulfuric acid, isopropyl alcohol, hydrochloric acid and ammonia were purchased from Merck Co., Germany. The analytical grade of chemicals was employed in this study and no purification was done prior to their use. The acetonitrile and methanol purchased from Chemlab Co., (Belgium) were of HPLC grade. HPLC grade water was used to prepare the stock solutions and BPS measurements.

2.2. Synthesis of nanocatalysts

2.2.1. Preparation of SBA-15 and Fe-SBA-15

SBA-15 was synthesized by hydrothermal method and tetraethyl orthosilicate (TEOS) was used as silica source as described by Zhao et al. [39].

Fe-SBA-15 nanocatalyst was prepared by an incipient wetness impregnation method using $Fe(NO_3)_3{\cdot}9H_2O$ as iron

source [40]. In order to prepare the Fe-SBA-15, initially, the SBA-15 was activated. For this purpose, the SBA-15 was submerged in 0.1 mol L^{-1} HCl for 24 h, and then, was filtered and was rinsed with distilled water and dried in a vacuum oven at 100°C for 8 h. A certain amount of $Fe(NO_3)_3 \cdot 9H_2O$ was dissolved in distilled water to prepare a solution of 1 mol L^{-1}. A sample of 1 g of SBA-15 was dispersed into the prepared solution by ultrasonication for 30 min. The obtained mixture was filtered and was dried at 100°C and was calcined at 750°C for 3 h. Thus, iron doped SBA-15 (Fe-SBA-15) was obtained.

2.2.2. Characterization of synthesized Fe-SBA-15

The as-synthesized Fe-SBA-15 was characterized by X-ray diffraction (XRD) on a PW1730 X-ray diffractometer (Philips, Netherlands) using Cu-Kα1 (λ = 1.54 Å) radiation at 40 kV and 30 mA. The diffractograms were recorded in the 2θ range of 0.5°–5° with a 2θ step size of 0.01°.

The specific surface area of the synthesized Fe-SBA-15 was calculated according to the Brunaur–Emmett–Teller method, and pore size distribution curves were obtained from the analysis of nitrogen adsorption isotherms using Barrett–Joyner–Halenda method on a BELSORP MINI II (Japan) at –196°C (77°K). Before each measurement, the sample was heated under vacuum at 450°C. A transmission electron microscope (TEM, Zeiss EM900, Germany) at 100 keV was used to identify the morphology of Fe-SBA-15. Bulk elemental analysis was performed by energy dispersive X-ray spectroscopy (EDX) (MIRA III TESCAN, Czech Republic). Fourier transform infrared spectroscopy (FTIR) analysis was carried out on a Shimadzu FTIR-8400S (Japan), using the KBr pellet and recording the spectra in the wavenumber range of 400–4,000 cm^{-1}.

2.3. Catalytic oxidation experiments procedure

All experiments were taken place in 500 mL pyrex beaker filled with 300 mL of BPS solution. Before the hybrid AOPs experiments, to perform the adsorption–desorption equilibrium behavior between the BPS and Fe-SBA-15 under a dark condition, a series of batch experiments were carried out. After reaching the adsorption equilibrium state between the Fe-SBA-15 and BPS in the suspension, the catalytic oxidation of BPS was accomplished by addition of PMS to the reaction solution. Finally, in hybrid AOPs reactions, MP UV lamp and ultrasonic bath were used to determine the effect of ultraviolet and ultrasound irradiation as PMS activator for BPS degradation (marked as Fe-SBA-15/UV/US/PMS system).

Schematic of the studied system is represented in Fig. 1. It consists of an ultrasonic bath procured from BANDELIN electronic GmbH, Berlin, Germany. Bath inner dimension was 300 mm°× 150°mm × 150 mm, l × w × d, electric power output was 80 W, fixed frequency of operation was 35 kHz and operating volume of the bath was 3.8 L. The temperature of the solution was fixed at 25°C by circulating the cooling water. A medium pressure UV lamp 125 W placed at a distance of 3 cm of solution as an ultraviolet radiation source to start the photolysis reactions. A digital laboratory overhead stirrer was used at 100 rpm for mixing the solution. At selected time intervals, 1.5 mL of the reaction solution was

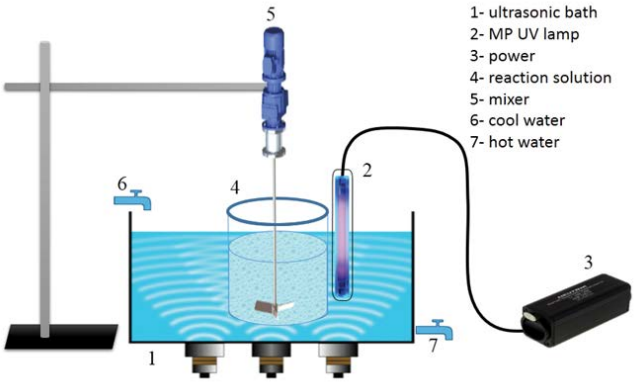

Fig. 1. Schematic diagram of the experimental setup used in this study.

taken from the reactor. After adding the 0.5 mL of methanol as a radical scavenger centrifuged, filtered through 0.45 μm membranes and injected into a micro tube. The remaining concentration of BPS was determined by high-performance liquid chromatography (HPLC). The effects of various parameters, such as the amount of nanocatalyst, initial pH values, initial concentration BPS and PMS on the BPS degradation kinetics were studied. Most experiments were done in duplicate and mean values (with standard deviation less than 5%) were reported as final result. The biodegradability of the BPS and the treated end solutions were analyzed as BOD_5. Recycling experiments were carried out to evaluate the reusability and stability of the Fe-SBA-15 nanocatalyst.

2.4. Apparatus and samples analysis

Separation and quantification of BPS were carried out using an HPLC V7603 system, manufactured by Knauer (Knauer, Germany) equipped with an ultimate variable wavelength UV detector (2500) and Shimadzu RF-10AXL fluorescence detector. A Nucleosil 100-5 C18 (250 mm°× 4.6 mm, 5 μm; Macherey-Nagel, Duren, Germany) was used to separate the target analytes.

The mobile phase was methanol: water +0.1% acetic acid (60:40) with a flow rate of 1.0 mL min^{-1} while the injection volume was 20 μL. The wavelengths of the UV detector were set at 255 nm and the retention time of BPS was 10 min. Data acquisition was performed using ChromGate Data System software (V 3.3.2). The limit of detection was 10 μg L^{-1}, whereas the limit of quantitation was 100 μg L^{-1}.

Stock solutions of 1,000 mg L^{-1} for BPS were prepared in methanol and kept at 4°C. Working standards were prepared by diluting the stock solutions. For the external calibration analytical curve, 10 points were used in the concentration range of 100 μg L^{-1}–5 mg L^{-1}. Each standard concentration was injected three times. All standard solutions and eluents were immediately filtered through syringe filter (0.22 μm pore size) prior to injection into the HPLC system.

The mineralization rate in terms of total organic carbon (TOC) and chemical oxygen demand (COD) abatement was evaluated by using a TOC analyzer (model Analytik Jena multi N/C 3100, Germany) and colorimetric method (5220-D) [41], respectively.

The measurement of the 5 d biochemical oxygen demand (BOD_5, mg L^{-1} O_2) was performed in a HACH BOD system thermostated at 20°C and using 500 mL bottles (HACH, USA).

Activated sludge inhibition tests were used to toxicity assessment of samples (before and after treatments). Inhibition of oxygen consumption (I_{OUR}) was measured based on Eq. (1).

$$I_{OUR}(\%) = [1 - (OUR_B - OUR_S)] \times 100 \quad (1)$$

where OUR_B and OUR_S are the OUR in the blank control and the test sample, respectively.

3. Results

3.1. Characterization of catalysts

The low-angle XRD patterns of the SBA-15 and Fe-SBA-15 samples were represented in Fig. 2. Obtained patterns were observed to be similar to SBA-15 materials [42,43]. The narrow (100) peaks at about 2θ = 0.9° for SBA-15 and Fe-SBA-15 were representative of the mesoporous structure and high orderings of the samples. Also, weak (110) and (200) peaks at 2θ = 1.5° and 1.7° shows the two-dimensional hexagonal structure of the samples. Considering the Fig. 2, no change was appeared in the XRD patterns of SBA-15 and Fe-SBA-15, except for the gradual reduction in diffraction intensity of Fe-SBA-15 than the SBA-15.

Fig. 3 determines the N_2 adsorption–desorption isotherm for studied samples at 77°K. Based on the IUPAC classification, the isotherms of both SBA-15 and Fe-SBA-15 are of type IV and it illustrates that these are placed in groups of the large pore mesoporous materials. The incorporation of Fe into the SBA-15 walls has a significant effect on the specific surface area and pore volume of the materials. The pore volume decreases from 0.991 to 0.862 cm^3 g^{-1} and the specific surface area declines from 777.89 to 710.25 m^2 g^{-1} (Table 1). Reduction in the pore volume might be due to the blocking of micropores and mesopores channels with iron during the calcination [43,44]. Table 1 shows the determined textural properties of the nitrogen sorption analysis.

EDX was employed to estimate the amount of iron introduced into channels of Fe-SBA-15. As shown in Fig. 4, EDX confirmed the existence of Fe with bulk loadings of 4.6 wt.%.

In the Fig. 5, TEM images of SBA-15 and Fe-SBA-15 were represented. TEM images of the mentioned samples reveal that there is no evident change in morphology and both of them are present as a short rod-like morphology. Fig. 5 confirms that the structure order of the Fe-SBA-15 is maintained even after the grafting procedure and immobilization of iron nanoparticles on the SBA-15 mesopores. The Fe nanoparticles appear as black dot-like objects between the mesopores channels.

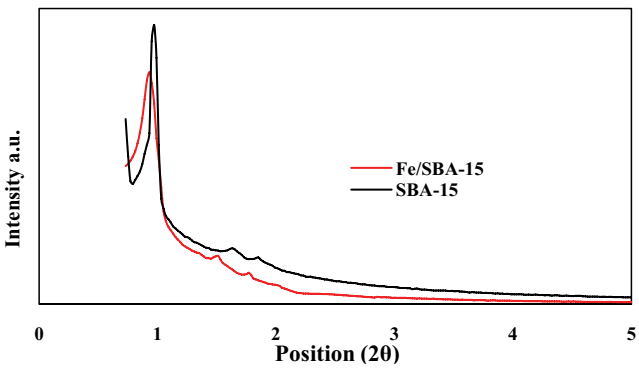

Fig. 2. Small-angle XRD patterns of SBA-15 and Fe-SBA-15.

Fig. 6 reveals the IR spectra of SBA-15 and Fe-SBA-15. For mesoporous SBA-15, the peaks at 1,150; 820 and 480 cm^{-1} were attributed to the asymmetric stretching, bending and rocking modes of Si–O–Si bond. The wide peak at 3,400 cm^{-1} was the characteristic peak of Si–OH bonds. Since there is no peak corresponds to the C–H vibrations at 2,850–3,000 cm^{-1}, it can be concluded that the surfactant is well removed. The FTIR studies of Fe-SBA-15 confirm that there was no change in functional group after the immobilization of iron nanoparticles on the SBA-15 mesopore. These findings are consistent with the results of other researchers [42,43,45].

3.2. BPS removal under different systems

In order to compare the different systems for BPS removal, 20 mg L^{-1} BPS was treated for 60 min by US and UV alone, US and UV, PMS alone, PMS and UV, PMS and US, PMS and UV and US, Fe-SBA-15 alone, SBA-15 alone, Fe-SBA-15 and PMS, Fe-SBA-15 and PMS and US, Fe-SBA-15 and PMS and UV, Fe-SBA-15 and PMS and US and UV process. BPS removal efficiencies represented in Fig. 7 were achieved by different systems under similar experimental conditions. BPS removal efficiencies by US alone, UV alone and PMS alone were only 9%, 5% and 6%, respectively, but removal efficiencies by UV and US, UV and PMS, PMS and US, PMS and UV and US were 17%, 30%, 28% and 43%, respectively. As expected, the BPS removal efficiencies of simultaneous processes are noticeably higher than individual systems. When US, UV and PMS were coupled with each other, the higher efficiencies were obtained. The reason for higher efficiencies could be attributed to the formation of reactive species ($OH^{\bullet}$ and $SO_4^{\bullet-}$ radicals) in binary or ternary systems, which plays important roles in the decomposition of organic contaminants. For understanding the BPS adsorption behavior on Fe-SBA-15 and its modeling, kinetics and isotherms studies were performed before the hybrid AOPs. It was observed that, during the initial times (t < 60 min), the adsorption rate was very rapid and then, there was no significant changes for the subsequent times. Therefore, it can be concluded that the adsorption process reached the equilibrium in the first 60 min of the experiment. So, prior to conducting the hybrid AOPs, the experiments in dark conditions were carried out for 60 min. The constant values of kinetic and equilibrium models of BPS adsorption are given in Table 2. Based on the results, BPS adsorption onto Fe-SBA-15 followed the pseudo-second-order and Freundlich models. The highest BPS adsorption capacity (q_0) of Fe-SBA-15 obtained from Langmuir model was 221.5 mg g^{-1}. For comparison, in the study of Wang et al. [46] the adsorption of Pb^{2+} on Fe_3O_4@SBA-15-NH2 was 149.2 mg g^{-1} at room temperature, in the study of Zhang et al. [47] the adsorption of tetracycline onto amino–Fe^{3+} functionalized SBA-15 was investigated and Q_{max} was 188 mmol kg^{-1} and also, in the

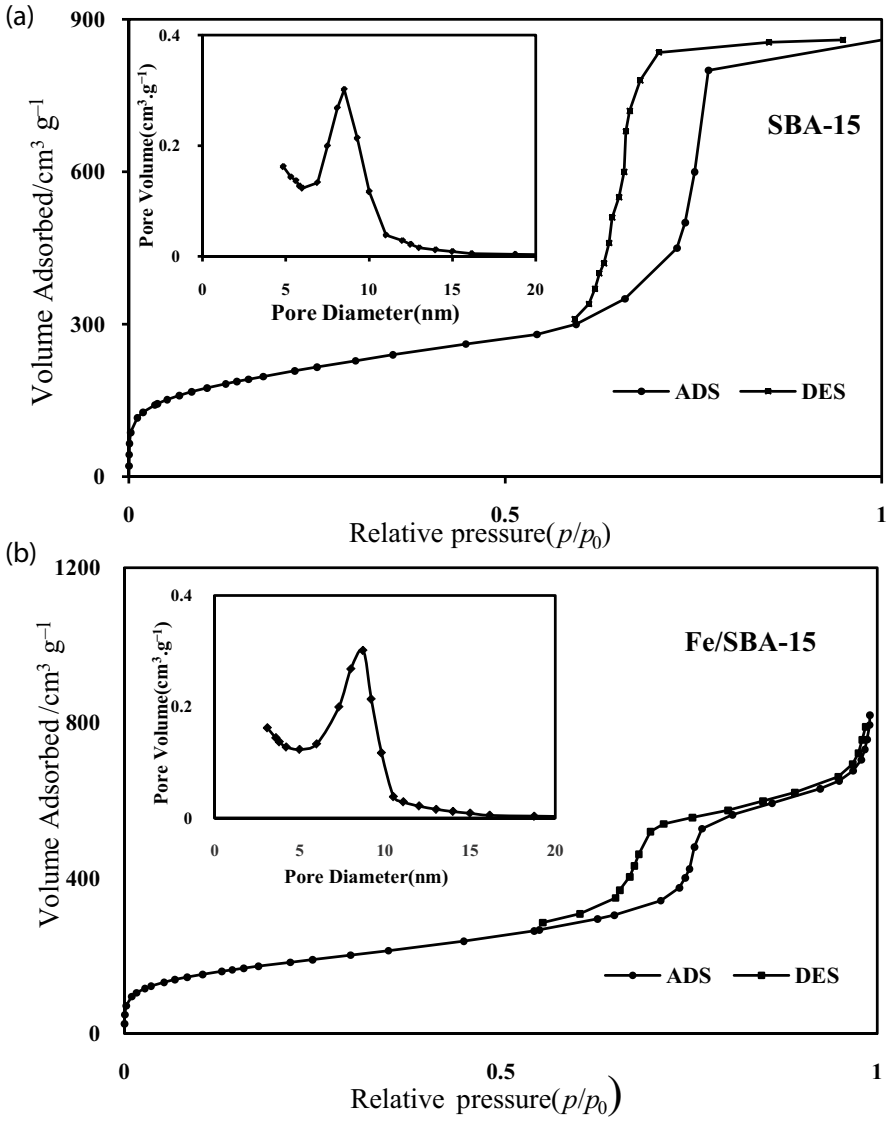

Fig. 3. Nitrogen adsorption–desorption isotherms and pore-size distribution (PSD) for SBA-15 and Fe-SBA-15.

Table 1
Textural properties of samples as calculated from nitrogen adsorption/desorption isotherms and cell parameters

Sample	S_{BET} ($m^2 g^{-1}$)	V_{meso} ($cm^3 g^{-1}$)[a]	V_{micro} ($cm^3 g^{-1}$)	d_0 (nm)
SBA-15	777.89	0.94	0.051	9.28
Fe-SBA-15	710.25	0.83	0.032	8.71

[a]$V_{meso} = V_{total} - V_{micro}$.

study of Guo et al. [48] the maximum adsorption capacity of functionalized SBA-15 with triglycine for Co(II) at 25°C obtained 181.67 mg g^{-1}.

According to Fig. 7, by simultaneous use of the US and UV and PMS, BPS removal reached 43%, but the BPS removal efficiency was observed to be 54% when the Fe-SBA-15 alone was used for activation of PMS. This shows that the use of Fe-SBA-15 alone is more effective than the simultaneous use of UV and US for PMS activation and the

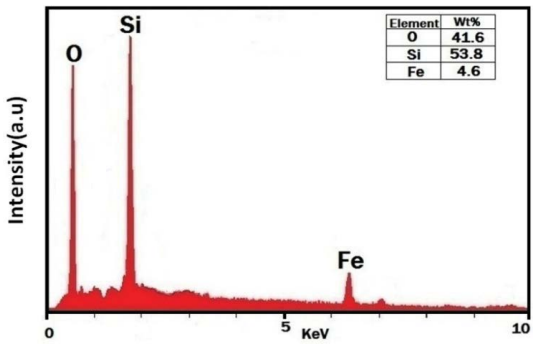

Fig. 4. EDX image of Fe-SBA-15 catalyst.

prepared Fe-SBA-15 has high capability to activating the PMS. Moreover, the application of Fe/SBA-15&PMS&US and Fe/SBA-15&PMS&UV provides the BPS removal efficiencies of 77% and 84%, respectively. This is explained by

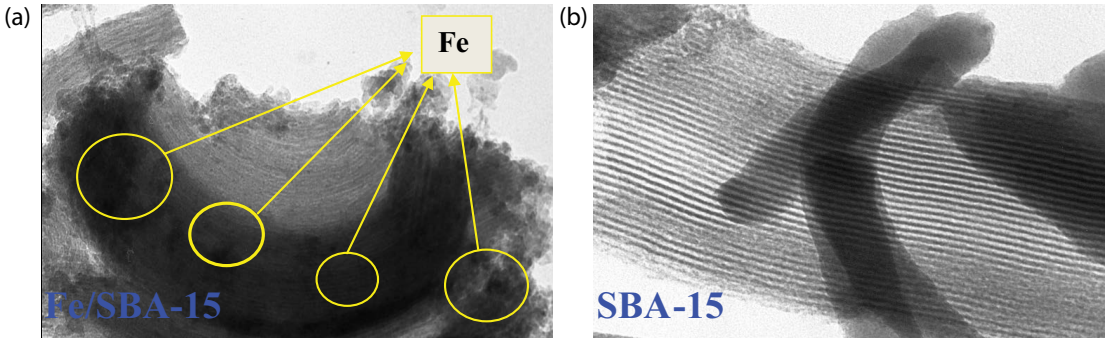

Fig. 5. TEM images of SBA-15 and Fe-SBA-15.

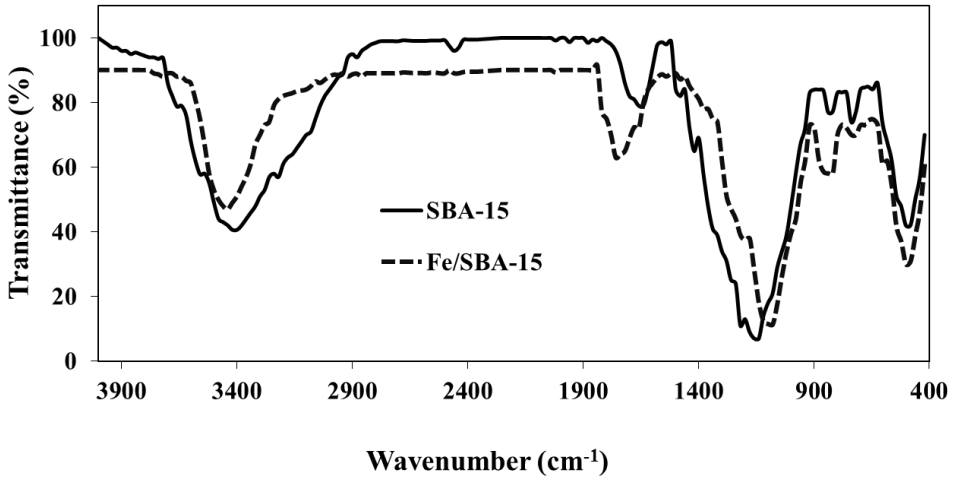

Fig. 6. IR spectra of SBA-15 and Fe-SBA-15.

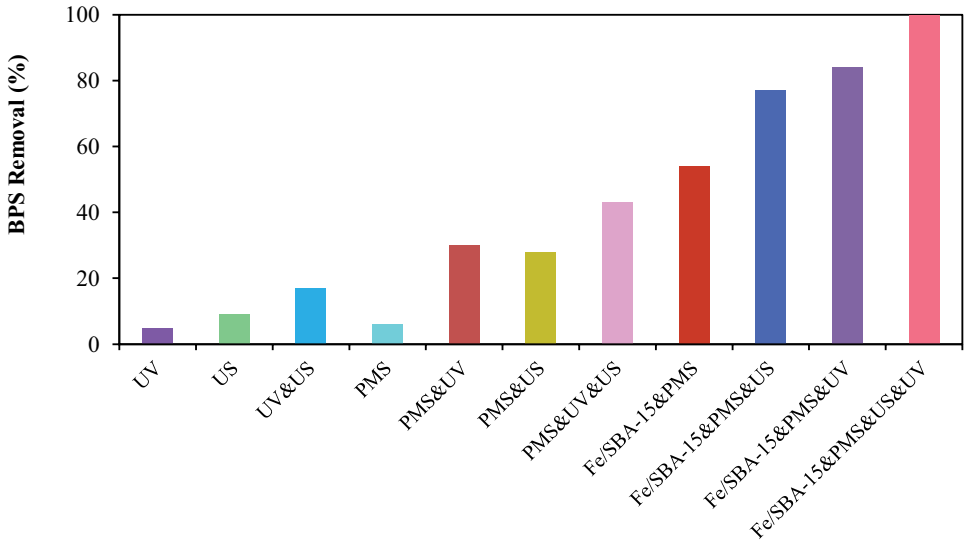

Fig. 7. Removal of BPS under various processes (reaction conditions: pH 7, 0.3 g L^{-1} catalyst (Fe-SBA-15); 3 mmol L^{-1} PMS, 80 W and 35 kHz ultrasonic power and frequency, 125 W MP UV irradiation, 20 mg L^{-1} BPS and 60 min reaction time).

this fact that both UV and US have important role in the decomposition of PMS and generation of the free radicals (i.e., $OH^{\bullet}$ and $SO_4^{\bullet-}$). As seen, the complete BPS degradation was obtained when Fe-SBA-15, PMS, UV and US were used simultaneously. This high efficiency indicates the synergistic effect of the active agents in the PMS decomposition and, which it is resulted in the formation of reactive oxidizing species. The comparison of the studied systems illustrated

Table 2
Kinetics and isotherms of BPS adsorption on Fe-SBA-15*

Parameters of the pseudo-second-order for BPS adsorption onto Fe-SBA-15					
q_e (mg g^{-1})		k_2 (g mg^{-1} min)		R^2	
101.6		0.0051		0.99	
Parameters of adsorption isotherms modeled by the Langmuir equation and Freundlich equation					
Langmuir			Freundlich		
q_m (mg g^{-1})	K_L (L mg^{-1})	R^2	K_F (mg (L mg^{-1})$^{1/2}$ g^{-1})	$1/n$	R^2
221.5	0.16	0.96	95.8	0.47	0.98

*These results are related to adsorption studies.

that the simultaneous use of Fe-SBA-15, UV and US for PMS activation is the best system for BPS degradation. Therefore, this system was selected as the best process to continue the optimization of BPS degradation.

3.3. Effect of the experimental conditions on BPS degradation

3.3.1. Effect of pH

The solution pH has a great effect on the formation and concentration of radicals in $SO_4^{\bullet-}$ based AOPs [20]. In order to investigate the effect of initial pH on BPS removal by Fe-SBA-15/UV/US/PMS process, the experiments were carried out at five initial pH values of BPS solution (pH_0: 3.2, 5.5, 7.0, 8.5 and 10.8). Within the 45 min, the removal efficiencies of 95%, 96%, 92%, 79% and 53% were obtained for pH values of 3.2, 5.5, 7, 8.5 and 10.8, respectively. As shown in Fig. 8, the performance of system under acidic and natural conditions was better than the alkaline conditions. Meanwhile, as shown in Fig. 8, no significant changes were observed in the removal efficiencies achieved at pH < 7.0. By increasing the solution pH from 3.2 to 10.8, observed degradation rate (k_1) decreased from 7.4 × 10^{-2} to 1.7 × 10^{-2} min^{-1}. One justification for this is that the removal efficiency is greater in the acidic and neutral conditions; in this case, the solubility of iron is higher, and additional iron provides better PMS decomposition, which it results in an increase in BPS oxidation rate.

Reducing the efficacy of BPS removal in alkaline pH (>7) may be due to the formation of Fe^{2+} complex Eq. (2), and the formation of this complex reduces the concentration of free Fe^{2+} [30].

$$Fe^{2+} + H_2O \rightarrow Fe(OH)^+ + H^+ \quad (2)$$

Also, according to Eq. (3), Fe^{3+} may be formed, and may precipitate in the formation of $Fe(OH)_3$, and eventually, precipitation may prevent the UV penetration and free radical generation [49].

$$Fe^{2+} + HSO_5^- \rightarrow Fe^{3+} + SO_4^{\bullet-} + OH^- \quad (3)$$

In strong alkaline conditions (pH > 8.5), according to Eq. (4), hydroxyl radical will produce, in these conditions, the rate of pollutants degradation will be slower [50].

$$SO_4^{\bullet-} + OH^- \rightarrow SO_4^{2-} + HO^{\bullet} \quad (4)$$

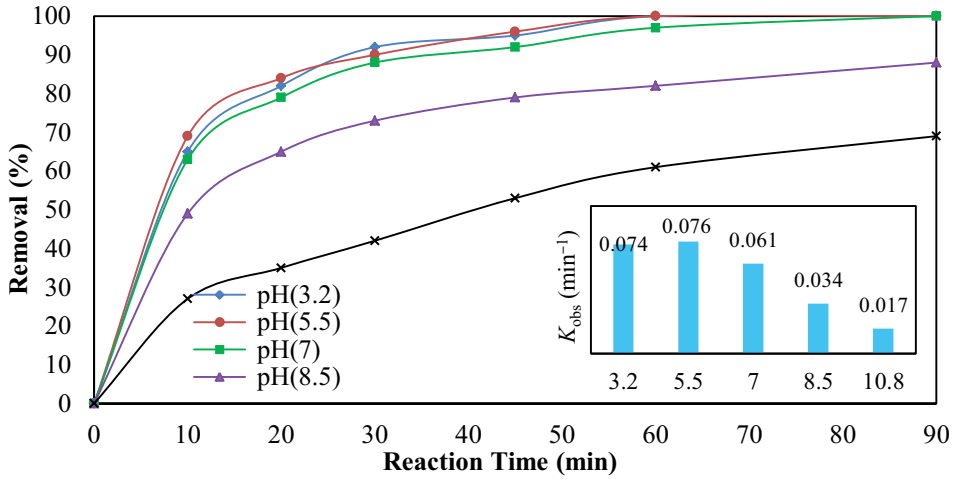

Fig. 8. Effect of solution pH on BPS degradation by hybrid AOPs (Fe-SBA-15/UV/US/PMS process) (reaction conditions: 0.3 g L–1 catalyst (Fe-SBA-15); 3 mmol L^{-1} PMS, 80 W and 35 kHz ultrasonic power and frequency, 125 W MP UV irradiation, 20 mg L^{-1} BPS and reaction time of 90 min).

It was proven that, at the solution pH < 7.0 and >9.0, the dominant radicals are $SO_4^{\bullet-}$ and $OH^{\bullet}$ and since the oxidation potential of $SO_4^{\bullet-}$ radicals is greater than $OH^{\bullet}$ radicals, the higher efficiency can occur at pH < 7.0 [51,52]. Similar results have been reported for sulfate-based AOPs for degradation of different contaminants [21,53,54].

It has already been mentioned that no significant changes were observed in the removal efficiencies of BPS achieved at pH < 7.0; therefore, taking into account the technical and economic conditions, the pH = 7.0 was selected as an optimum value for conducting the subsequent experiments. The results of this study show that the Fe-SBA-15/UV/US/PMS hybrid process has a good activity for the degradation of BPS without any pH adjustment.

3.3.2. Effect of PMS concentration

BPS degradation in Fe-SBA-15/UV/US/PMS system was done at the PMS concentration of 0.5–4 mmol L^{-1}. As shown in Fig. 9, the reaction speed is initially high, and then, it reduces. Moreover, by increasing the amount of PMS from 0.5 to 3 mmol L^{-1}, the BPS degradation efficiency increased from 76% to 100%. The degradation of BPS in this system can be explained by the first order reaction kinetics ($\ln(C/C_0) = -kt$). The rate constant of BPS degradation was improved from 1.7×10^{-2} to 6.2×10^{-2} min^{-1} by increasing the amount of PMS from 0.5 to 3 mmol L^{-1}. The efficiency of BPS degradation was not changed by increasing the amount of PMS from 3 to 4 mmol L^{-1}; and hence, 3 mmol L^{-1} was utilized as the optimum condition in next steps of study. Other studies also emphasized that rising the amount of PMS could not continuously improve the degradation of pollutant [55–57]. This may be due to: (i) $SO_4^{\bullet-}$ and $OH^{\bullet}$ may be combined again, Eqs. (5) and (6); (ii) the reaction between the above radicals may occur, Eq. (7); (iii) the scavenging reactions for PMS may happen, Eqs. (8) and (9).

$$SO_4^{\bullet-} + SO_4^{\bullet-} \rightarrow 2\,SO_4^{2-} \text{ or } S_2O_8^{2-} \quad (5)$$

$$OH^{\bullet} + OH^{\bullet} \rightarrow H_2O_2 \quad (6)$$

$$SO_4^{\bullet-} + OH^{\bullet} \rightarrow HSO_4^{-} + 1/2\,O_2 \quad (7)$$

$$HSO_5^{-} + SO_4^{\bullet-} \rightarrow SO_5^{\bullet-} + SO_4^{2-} + H^{+} \quad (8)$$

$$HSO_5^{-} + OH^{\bullet} \rightarrow SO_5^{\bullet-} + H_2O \text{ or } HSO_4^{-} + HO_2^{\bullet} \quad (9)$$

Similar results have been obtained by the study conducted by Ji et al. [58], who used the iron and UV for activation of PMS to the degradation of 2,4,5-trichlorophenoxy acetic acid.

3.3.3. Effect of Fe-SBA-15 dosage

Studying the influence dosage variation on the BPS degradation in Fe-SBA-15/UV/US/PMS system was carried out using the Fe-SBA-15 dosages in the range of 100–500 mg L^{-1}. Due to the presence of iron in Fe-SBA-15 channels that plays an important role in the activation of PMS, the catalyst dosage would significantly affect the degradation efficiency. As shown in Fig. 10, by increasing the catalyst dosage from 100 to 300 mg L^{-1}, the degradation efficiency of BPS was increased from 75% to 100%, and the rate constant was increased from 1.8×10^{-2} to 7.6×10^{-2} min^{-1}. According to Fig. 10, the BPS degradation efficiency for catalyst amount higher than 300 mg L^{-1} has not been significantly changed. So, due to technical and economic factors, 300 mg L^{-1} was selected in the next experiments.

3.3.4. Effect of initial BPS concentration

To evaluate the efficiency of this method, the BPS was degraded at concentration of 10–50 mg L^{-1} in Fe-SBA-15/UV/US/PMS system. Fig. 11 indicates that the degradation rate was decreased by an increase in initial BPS concentration from 10 to 50 mg L^{-1}. As long as the initial concentration of BPS was less than 20 mg L^{-1}, the complete removal of BPS was achieved during 60 min reaction. However, during the

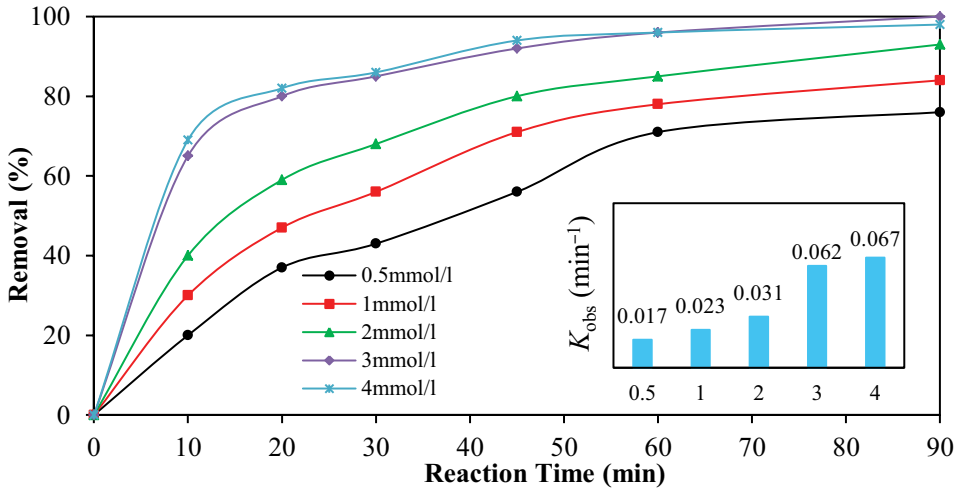

Fig. 9. Effect of PMS dosage on the BPS degradation by hybrid AOPs (Fe-SBA-15/UV/US/PMS process) (reaction conditions: pH 7, 0.3 g L^{-1} catalyst (Fe-SBA-15), 80 W and 35 kHz ultrasonic power and frequency, 125 W MP UV irradiation, 20 mg L^{-1} BPS and 90 min reaction time).

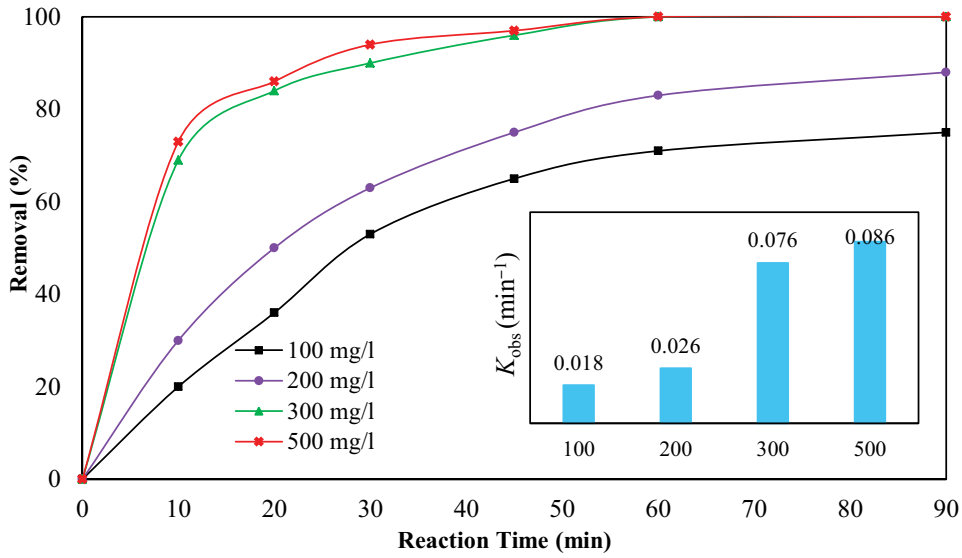

Fig. 10. Effect of catalyst loading on BPS degradation by hybrid AOPs (Fe-SBA-15/UV/US/PMS process) (reaction conditions: pH 7, 3 mmol L^{-1} PMS, 80 W and 35 kHz ultrasonic power and frequency, 125 W MP UV irradiation, 20 mg L^{-1} BPS and 90 min reaction time).

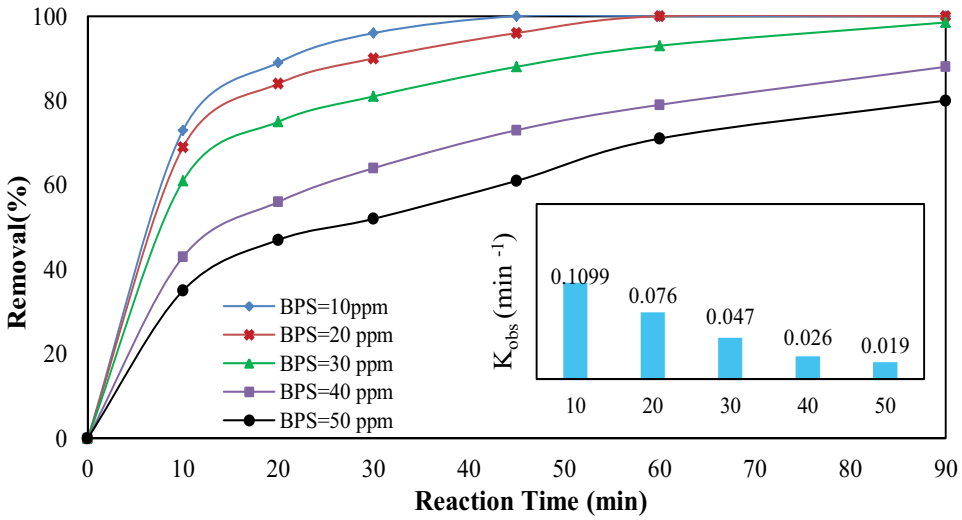

Fig. 11. Effect of initial BPS concentration on BPS degradation by hybrid AOPs (Fe-SBA-15/UV/US/PMS process) (reaction conditions: pH 7, 0.3 g L^{-1} catalyst (Fe-SBA-15), 3 mmol L^{-1} PMS, 80 W and 35 kHz ultrasonic power and frequency, 125 W MP UV irradiation and 90 min reaction time).

reaction time of 90 min, the removal efficiencies of 98.5%, 88% and 80% were obtained for BPS concentrations of 30, 40 and 50 mg L^{-1}, respectively. Also, the reaction rate constant for initial BPS concentration of 10 and 50 mg L^{-1} was 10.9×10^{-2} and 1.9×10^{-2} min^{-1}, respectively and this is consistent with the literature [17,38]. Under the similar conditions, except for initial BPS concentration, the amount of generated radicals appears to be constant. Therefore, the probability of reaction between the reactive species and BPS molecules would be decreased by increasing the BPS concentration. Another reason is this fact that the produced intermediates might compete with the main molecules for the reaction with reactive species [16,59,60].

3.4. Recyclability and durability of Fe-SBA-15 in activation of PMS

The recyclability and durability of the catalysts are very critical factors to estimate their cost-effectiveness estimation. The consecutive experiments were performed to investigate the Fe-SBA-15 stability. Both recyclability and durability of Fe-SBA-15 during Fe-SBA-15/UV/US/PMS system under optimum conditions were tested in multiple cycles. As displayed in Fig. 12, after five cycles, a slight drop (<6%) was observed in BPS removal efficiency by the studied system; so that, the BPS removal efficiencies of 100% and 94.2% were achieved for first and fifth cycles within the reaction time of

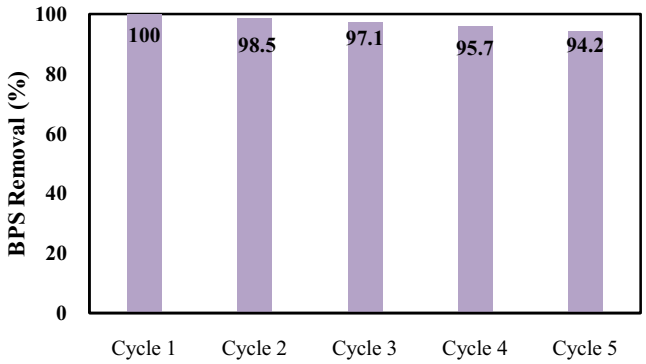

Fig. 12. Recycling tests in the Fe-SBA-15/UV/US/PMS system under optimum conditions (reaction conditions: pH 7, 0.3 g L^{-1} catalyst (Fe-SBA-15), 3 mmol L^{-1} PMS, 80 W and 35 kHz ultrasonic power and frequency, 125 W MP UV irradiation, 20 mg L^{-1} BPS and 60 min reaction time).

60 min, respectively. Also, the durability of the as-synthesized catalyst was assessed by measuring the iron leaching from Fe-SBA-15 into the solution reaction. The iron loss was measured to be lower than 0.2% for all cycles, which shows that the studied catalyst has a high physicochemical stability and iron species have been forcefully attached to the mesoporous channels. These results show that Fe-SBA-15 has a good reusability potential and can be reused for at least five cycles with high efficiency (>94%).

3.5. Scavenging tests

Two dominant radical species that may form in this system include $SO_4^{\bullet-}$ and $OH^{\bullet}$. In order to confirm the role of the dominant oxidizing radical species, two scavengers of ethanol and *t*-butanol were selected for this purpose. Ethanol (from group alpha hydrogen containing alcohols) is capable of scavenging both $SO_4^{\bullet-}$ and $OH^{\bullet}$ with rate constants of 1.6–7.7 × 10^7 M^{-1} s^{-1} and 1.2–2.8 × 10^9 M^{-1} s^{-1}, respectively [61]. As shown in Fig. 13, the removal efficiency of BPS by Fe-SBA-15/UV/US/PMS system decreased from 100% to 17.6% in the presence of 0.5 M ethanol. Considering the results, both hydroxyl and sulfate radicals were essential and played an imperative role in the BPS degradation. tert-Butanol is often used as a scavenger for hydroxyl radical because its rate constant is 418–1,900 times greater (rate constant = 3.8–7.6 × 10^8 M^{-1} s^{-1}) than sulfate radical (rate constant = 4–9.1 × 10^5 M^{-1} s^{-1}) [16,61]. As depicted in Fig. 13, by addition of 0.5 M *t*-butanol, the removal efficiency of BPS by Fe-SBA-15/UV/US/PMS system was reduced from 100% to 77.8%. It can be concluded that the dominant radicals in Fe-SBA-15/UV/US/PMS system are sulfate radicals.

3.6. Degradation mechanism under Fe-SBA-15/UV/US/PMS system

Based on the results and literature, a possible mechanism for hybrid PMS activation system (Fe-SBA-15/UV/US/PMS) is proposed in Fig. 14. This figure is based on participation of both adsorption on the surfaces of the Fe/SBA-15 and oxidation in BPS degradation. In solid phase, BPS and PMS molecules absorbed on the Fe/SBA-15 surface. The effective contact between the BPS and PMS increases the rate of degradation on the catalyst surface. The production of active species ($SO_4^{\bullet-}$, $SO_5^{\bullet-}$ and $OH^{\bullet}$) is done through the reaction between PMS and Fe^{2+}/Fe^{3+} ions both on the catalyst surfaces and in the solution. Also, BPS degradation rate in the liquid phase and solid phase accelerates by further decomposition of PMS by UV and US radiations by generation of further $SO_4^{\bullet-}$ and $OH^{\bullet}$. Accordingly, due to the synergistic effect between oxidation and adsorption processes, catalytic degradation of BPS has been considerably enhanced in Fe-SBA-15/UV/US/PMS system. Overall, due to the simultaneous presence of active species and significant production rate of $SO_4^{\bullet-}$ and $OH^{\bullet}$ radicals because of three activators; UV light, US irradiation and Fe/SBA-15 nanocatalyst were involved in PMS activation during Fe-SBA-15/UV/US/PMS system, therefore, this system can represent a high degradation efficiency for organic pollutants [16,38].

3.7. Mineralization and toxicity assessment experiments

As shown in Fig. 15, at the optimal conditions, the mineralization degree in Fe-SBA-15/UV/US/PMS system was 67% over 60 min of reaction. The reason for incomplete removal of TOC, despite the complete removal of BPS, is this fact that removal of produced intermediates is more difficult and their complete removal, compared with the main molecule, requires more oxidation. Activated sludge inhibition experiment was used for toxicity assessment of the treatment method. As shown in Fig. 15, the I_{OUR} value of the initial BPS solution was 25%. This trend has been enhanced up to 10 min after the initial reaction, which shows that the toxicity of intermediates is higher than that of BPS. Then, this trend rate declined and it reached 0.04% after 60 min of reaction time. These results indicated that Fe-SBA-15/UV/US/PMS system is capable of removing the BPS and its intermediates effectively.

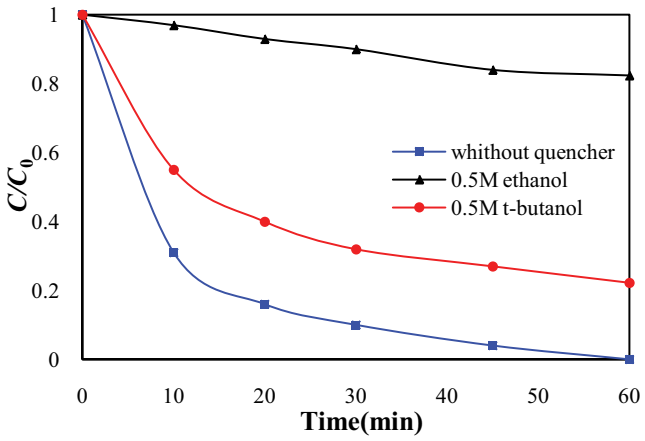

Fig. 13. Effect of scavengers on the degradation of BPS in the Fe-SBA-15/UV/US/PMS system under optimum conditions (reaction conditions: pH 7, 0.3 g L^{-1} catalyst [Fe-SBA-15], 3 mmol L^{-1} PMS, 80 W and 35 kHz ultrasonic power and frequency, 125 W MP UV irradiation, 20 mg L^{-1} BPS and 60 min reaction time).

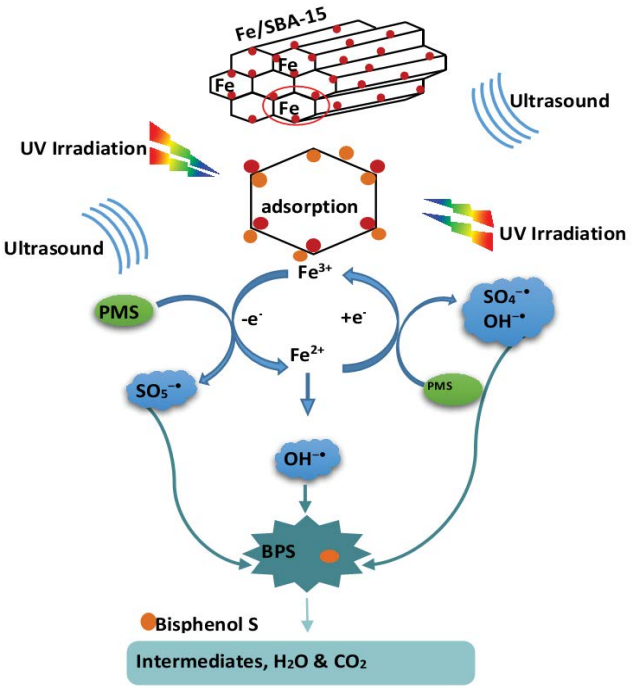

Fig. 14. BPS degradation under Fe-SBA-15/UV/US/PMS system.

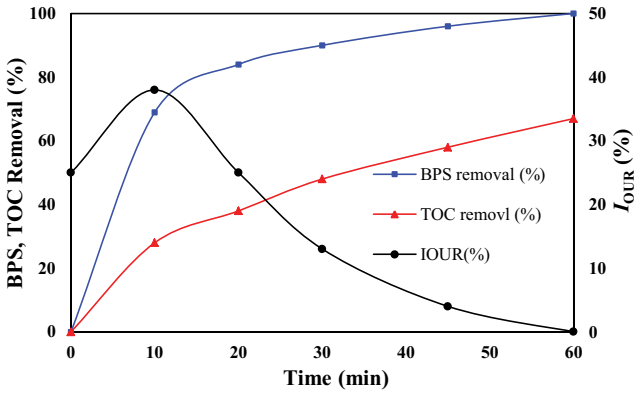

Fig. 15. Changes of BPS, TOC and I_{OUR} in the Fe-SBA-15/UV/US/PMS system under optimum conditions (reaction conditions: pH 7, 0.3 g L^{-1} catalyst (Fe-SBA-15), 3 mmol L^{-1} PMS, 80 W and 35 kHz ultrasonic power and frequency, 125 W MP UV irradiation, 20 mg L^{-1} BPS and 60 min reaction time).

3.8. Biodegradability of BPS

The biodegradability improvement of the wastewater is accounted for as an apt approach to assess the methods introduced for wastewater treatment. Evaluation of biodegradability was carried out based on BOD_5/COD ratio: biodegradable (>0.6), partially biodegradable (0.4–0.6) and nonbiodegradable (<0.4) [62]. Table 3 presents the biodegradability of different concentrations of BPS. The results of this study show that the solution with BPS concentration of 40 mg L^{-1} and above are not biodegradable, 30 mg L^{-1} is partially biodegradable and 20 mg L^{-1} and lower are totally biodegradable.

The biodegradability of samples was studied using the concentration of 50 mg L^{-1}. The determination of BOD_5 of samples was accomplished at different times (5–60 min) in Fe-SBA-15/UV/US/PMS system. Table 4 depicts the results

Table 3
Biodegradability of the BPS solutions in different concentrations

BPS (mg L^{-1})	TOC (mg L^{-1})	COD (mg L^{-1})	BOD_5	BOD_5/COD	Biodegradability
2	1.06	2.83	24	7.66	Yes
5	2.641	7.04	23	2.94	Yes
10	5.12	13.65	15.6	0.99	Yes
20	10.89	29.04	24	0.76	Yes
30	16.76	44.69	23	0.48	Partially
40	22.07	58.86	22	0.35	No
50	28.63	76.35	19	0.24	No

Table 4
Biodegradability improvement of BPS solution (50 mg L^{-1}) under optimum conditions

Time (min)	TOC (mg L^{-1})	COD (mg L^{-1})	BOD_5	BOD_5/COD	Biodegradability
0	28.63	76.35	19	0.24	No
5	33.2	88.3	11	0.12	No
10	38.6	102.9	8	0.07	No
20	26.85	71.6	20	0.27	No
30	19.42	51.8	22.4	0.43	No
45	12.7	34.1	20	0.58	No
60	9.51	11.24	24	2.14	yes

related to the biodegradability of samples at different times. As expected, there is no biodegradability in the samples studied at the initial steps of reaction due to the high concentrations of BPS and TOC; however, after 60 min, because of degrading the most of BPS and intermediates, the solution became biodegradable.

4. Conclusion

The synthesized Fe/SBA-15, as a heterogeneous catalyst, along with UV and US, illustrated a surprising capability for activation of the peroxymonosulfate and for degradation of bisphenol S. Moreover, it was clarified that simultaneous use of UV and US with Fe/SBA-15 has synergistic effect on activation of PMS and degradation of BPS. At the optimum condition, the BPS and TOC removal efficiencies at 60 min were obtained to be 100% and 67%, respectively.

In addition, the dependence of the efficiency of process studied on pH, PBS concentration and the dosage of catalyst and PMS was verified and the BPS degradation process follows the pseudo-first-order reactions. The initial I_{OUR} value for the 20 mg L^{-1} BPS solution was 25 and it was increased after 10 min which indicates that the intermediate compounds produced are more toxic; however, after 60 min, the I_{OUR} value reaches 0.04 which it reveals that toxicity of the BPS and intermediate compounds produced have been eliminated by this method. Furthermore, among different species of oxidizing radicals, the sulfate radical was found as dominant species in this system. Considering the results, simultaneous use of UV and US with Fe/SBA-15 is an effective way to activate PMS and to produce active radicals for sewage treatment.

Acknowledgment

The support of Hamadan University of Medical Sciences for this work (9610196620) is appreciated.

References

[1] C. Rousselle, J.N. Ormsby, B. Schaefer, A. Lampen, T. Platzek, K. Hirsch-Ernst, M. Warholm, A. Oskarsson, P.J. Nielsen, M.L. Holmer, C. Emond, Meeting report: international workshop on endocrine disruptors: exposure and potential impact on consumers health, Regul. Toxicol. Pharm., 65 (2013) 7–11.
[2] J.D. Meeker, Exposure to environmental endocrine disrupting compounds and men's health, Maturitas, 66 (2010) 236–241.
[3] M. Mezcua, M.A. Martínez-Uroz, M.M. Gómez-Ramos, M.J. Gómez, J.M. Navas, A.R. Fernández-Alba, Analysis of synthetic endocrine-disrupting chemicals in food: a review, Talanta, 100 (2012) 90–106.
[4] C.D. Bope, A. Nalaparaju, C.K. Ng, Y. Cheng, L. Lu, Molecular simulation on the interaction of Ethinylestradiol (EE2) with polymer membranes in wastewater purification, Mol. Simul., 44 (2018) 638–647.
[5] Z. Liu, N. Wardenier, S. Hosseinzadeh, Y. Verheust, P.-J. De Buyck, M. Chys, A. Nikiforov, C. Leys, S. Van Hulle, Degradation of bisphenol A by combining ozone with UV and H_2O_2 in aqueous solutions: mechanism and optimization, Clean Technol. Environ. Policy, 20 (2018) 2109–2118.
[6] B. Huang, D. Xiong, H. He, X. Li, W. Sun, X. Pan, Characteristics and bioaccumulation of Progestogens, Androgens, Estrogens, and Phenols in Erhai Lake Catchment, Yunnan, China, Environ. Eng. Sci., 34 (2017) 321–332.
[7] P. Shao, Z. Ren, J. Tian, S. Gao, X. Luo, W. Shi, B. Yan, J. Li, F. Cui, Silica hydrogel-mediated dissolution-recrystallization strategy for synthesis of ultrathin α-Fe_2O_3 nanosheets with highly exposed (1 1 0) facets: a superior photocatalyst for degradation of bisphenol S, Chem. Eng. J., 323 (2017) 64–73.
[8] J. Moreman, O. Lee, M. Trznadel, A. David, T. Kudoh, C.R. Tyler, Acute toxicity, teratogenic, and estrogenic effects of bisphenol A and its alternative replacements bisphenol S, bisphenol F, and bisphenol AF in zebrafish embryo-larvae, Environ. Sci. Technol., 51 (2017) 12796–12805.
[9] G. Cao, J. Lu, G. Wang, Photolysis kinetics and influencing factors of bisphenol S in aqueous solutions, J. Environ. Sci., 24 (2012) 846–851.
[10] G. Cao, R. He, Z. Cai, J. Liu, Photolysis of bisphenol S in aqueous solutions and the effects of different surfactants, React. Kinet. Mech. Catal., 109 (2013) 259–271.
[11] M.-Y. Chen, M. Ike, M. Fujita, Acute toxicity, mutagenicity, and estrogenicity of bisphenol-A and other bisphenols, Environ. Toxicol., 17 (2002) 80–86.
[12] P. Viñas, N. Campillo, N. Martínez-Castillo, M. Hernández-Córdoba, Comparison of two derivatization-based methods for solid-phase microextraction-gas chromatography-mass spectrometric determination of bisphenol A, bisphenol S and biphenol migrated from food cans, Anal. Bioanal. Chem., 397 (2010) 115–125.
[13] H.-B. Moon, S.-P. Yoon, R.-H. Jung, M. Choi, Wastewater treatment plants (WWTPs) as a source of sediment contamination by toxic organic pollutants and fecal sterols in a semi-enclosed bay in Korea, Chemosphere, 73 (2008) 880–889.
[14] F. Ghanbari, M. Moradi, Application of peroxymonosulfate and its activation methods for degradation of environmental organic pollutants, Chem. Eng. J., 310 (2017) 41–62.
[15] G. Sekaran, S. Karthikeyan, C. Evvie, R. Boopathy, P. Maharaja, Oxidation of refractory organics by heterogeneous Fenton to reduce organic load in tannery wastewater, Clean Technol. Environ. Policy, 15 (2013) 245–253.
[16] C. Cai, H. Zhang, X. Zhong, L. Hou, Ultrasound enhanced heterogeneous activation of peroxymonosulfate by a bimetallic Fe–Co/SBA-15 catalyst for the degradation of Orange II in water, J. Hazard. Mater., 283 (2015) 70–79.
[17] A.J. Jafari, B. Kakavandi, N. Jaafarzadeh, R.R. Kalantary, M. Ahmadi, A.A. Babaei, Fenton-like catalytic oxidation of tetracycline by AC@Fe_3O_4 as a heterogeneous persulfate activator: adsorption and degradation studies, J. Ind. Eng. Chem., 45 (2017) 323–333.
[18] J. Deng, M. Xu, S. Feng, C. Qiu, X. Li, J. Li, Iron-doped ordered mesoporous Co_3O_4 activation of peroxymonosulfate for ciprofloxacin degradation: performance, mechanism and degradation pathway, Sci. Total Environ., 658 (2019) 343–356.
[19] H. Hussain, I.R. Green, I. Ahmed, Journey describing applications of oxone in synthetic chemistry, Chem. Rev., 113 (2013) 3329–3371.
[20] Y.-H. Guan, J. Ma, X.-C. Li, J.-Y. Fang, L.-W. Chen, Influence of pH on the formation of sulfate and hydroxyl radicals in the UV/peroxymonosulfate system, Environ. Sci. Technol., 45 (2011) 9308–9314.
[21] J. Liu, J. Zhou, Z. Ding, Z. Zhao, X. Xu, Z. Fang, Ultrasound irritation enhanced heterogeneous activation of peroxymonosulfate with Fe_3O_4 for degradation of azo dye, Ultrason. Sonochem., 34 (2017) 953–959.
[22] S. Yang, P. Wang, X. Yang, L. Shan, W. Zhang, X. Shao, R. Niu, Degradation efficiencies of azo dye Acid Orange 7 by the interaction of heat, UV and anions with common oxidants: persulfate, peroxymonosulfate and hydrogen peroxide, J. Hazard. Mater., 179 (2010) 552–558.
[23] T. Zhang, H. Zhu, J.-P. Croue, Production of sulfate radical from peroxymonosulfate induced by a magnetically separable $CuFe_2O_4$ spinel in water: efficiency, stability, and mechanism, Environ. Sci. Technol., 47 (2013) 2784–2791.
[24] J. Deng, Y. Ge, C. Tan, H. Wang, Q. Li, S. Zhou, K. Zhang, Degradation of ciprofloxacin using α-MnO_2 activated peroxymonosulfate process: effect of water constituents, degradation intermediates and toxicity evaluation, Chem. Eng J., 330 (2017) 1390–1400.

[25] J. Deng, S. Feng, K. Zhang, J. Li, H. Wang, T. Zhang, X. Ma, Heterogeneous activation of peroxymonosulfate using ordered mesoporous Co_3O_4 for the degradation of chloramphenicol at neutral pH, Chem. Eng. J., 308 (2017) 505–515.
[26] C. Cai, H. Zhang, X. Zhong, L. Hou, Electrochemical enhanced heterogeneous activation of peroxydisulfate by Fe–Co/SBA-15 catalyst for the degradation of Orange II in water, Water Res., 66 (2014) 473–485.
[27] G.K. Dinesh, S. Anandan, T. Sivasankar, Synthesis of Fe-doped Bi_2O_3 nanocatalyst and its sonophotocatalytic activity on synthetic dye and real textile wastewater, Environ. Sci. Pollut. Res., 23 (2016) 20100–20110.
[28] N. Jaafarzadeh, M. Omidinasab, F. Ghanbari, Combined electrocoagulation and UV-based sulfate radical oxidation processes for treatment of pulp and paper wastewater, Process. Saf. Environ. Prot., 102 (2016) 462–472.
[29] Q. Chen, F. Ji, Q. Guo, J. Fan, X. Xu, Combination of heterogeneous Fenton-like reaction and photocatalysis using Co–TiO_2 nanocatalyst for activation of $KHSO_5$ with visible light irradiation at ambient conditions, J. Environ. Sci., 26 (2014) 2440–2450.
[30] S. Khan, X. He, H.M. Khan, D. Boccelli, D.D. Dionysiou, Efficient degradation of lindane in aqueous solution by iron (II) and/or UV activated peroxymonosulfate, J. Photochem. Photobiol., A, 316 (2016) 37–43.
[31] S. Su, W. Guo, C. Yi, Y. Leng, Z. Ma, Degradation of amoxicillin in aqueous solution using sulphate radicals under ultrasound irradiation, Ultrason. Sonochem., 19 (2012) 469–474.
[32] A. Shahbazi, H. Younesi, A. Badiei, Functionalized SBA-15 mesoporous silica by melamine-based dendrimer amines for adsorptive characteristics of Pb(II), Cu(II) and Cd(II) heavy metal ions in batch and fixed bed column, Chem. Eng. J., 168 (2011) 505–518.
[33] P. Xu, G.M. Zeng, D.L. Huang, C.L. Feng, S. Hu, M.H. Zhao, C. Lai, Z. Wei, C. Huang, G.X. Xie, Use of iron oxide nanomaterials in wastewater treatment: a review, Sci. Total Environ., 424 (2012) 1–10.
[34] A.B. Cundy, L. Hopkinson, R.L.D. Whitby, Use of iron-based technologies in contaminated land and groundwater remediation: a review, Sci. Total Environ., 400 (2008) 42–51.
[35] R. Jinisha, R. Gandhimathi, S.T. Ramesh, P.V. Nidheesh, S. Velmathi, Removal of rhodamine B dye from aqueous solution by electro-Fenton process using iron-doped mesoporous silica as a heterogeneous catalyst, Chemosphere, 200 (2018) 446–454.
[36] X. Sun, Y. Yan, J. Li, W. Han, L. Wang, SBA-15-incorporated nanoscale zero-valent iron particles for chromium(VI) removal from groundwater: mechanism, effect of pH, humic acid and sustained reactivity, J. Hazard. Mater., 266 (2014) 26–33.
[37] P. Shukla, S. Wang, H. Sun, H.-M. Ang, M. Tadé, Adsorption and heterogeneous advanced oxidation of phenolic contaminants using Fe loaded mesoporous SBA-15 and H_2O_2, Chem. Eng. J., 164 (2010) 255–260.
[38] A. Takdastan, B. Kakavandi, M. Azizi, M. Golshan, Efficient activation of peroxymonosulfate by using ferroferric oxide supported on carbon/UV/US system: a new approach into catalytic degradation of bisphenol A, Chem. Eng. J., 331 (2018) 729–743.
[39] D. Zhao, J. Feng, Q. Huo, N. Melosh, G.H. Fredrickson, B.F. Chmelka, G.D. Stucky, Triblock copolymer syntheses of mesoporous silica with periodic 50 to 300 angstrom pores, Science, 279 (1998) 548–552.
[40] R. Huang, H. Yan, L. Li, D. Deng, Y. Shu, Q. Zhang, Catalytic activity of Fe/SBA-15 for ozonation of dimethyl phthalate in aqueous solution, Appl. Catal., B, 106 (2011) 264–271.
[41] APHA, AWWA, Standard Methods for the Examination of Water and Wastewater, American Public Health Association, Washington, 1989.
[42] N.S. Sanjini, S. Velmathi, Iron impregnated SBA-15, a mild and efficient catalyst for the catalytic hydride transfer reduction of aromatic nitro compounds, RSC Adv., 4 (2014) 15381–15388.
[43] R. Ragavan, A. Pandurangan, Facile synthesis and super-capacitor performances of nitrogen doped CNTs grown over mesoporous Fe/SBA-15 catalyst, New J. Chem., 41 (2017) 11591–11599.
[44] A. Vinu, D.P. Sawant, K. Ariga, K.Z. Hossain, S.B. Halligudi, M. Hartmann, M. Nomura, Direct synthesis of well-ordered and unusually reactive FeSBA-15 mesoporous molecular sieves, Chem. Mater., 17 (2005) 5339–5345.
[45] S. Beirami, H.R. Barzoki, N. Bahramifar, Application of response surface methodology for optimization of trace amount of diazinon preconcentration in natural waters and biological samples by carbon mesoporous CMK-3, Biomed. Chromatogr., 31 (2017) 3874–3876.
[46] S. Wang, K. Wang, C. Dai, H. Shi, J. Li, Adsorption of Pb^{2+} on amino-functionalized core–shell magnetic mesoporous SBA-15 silica composite, Chem. Eng. J., 262 (2015) 897–903.
[47] Z. Zhang, H. Li, H. Liu, Insight into the adsorption of tetracycline onto amino and amino-Fe^{3+} gunctionalized mesoporous silica: effect of functionalized groups, J. Environ. Sci., 65 (2018) 171–178.
[48] W. Guo, R. Chen, Y. Liu, M. Meng, X. Meng, Z. Hu, Z. Song, Preparation of ion-imprinted mesoporous silica SBA-15 functionalized with triglycine for selective adsorption of Co(II), Colloids Surf., A, 436 (2013) 693–703.
[49] A. Stefánsson, Iron(III) hydrolysis and solubility at 25°C, Environ. Sci. Technol., 41 (2007) 6117–6123.
[50] Y. Ding, H. Tang, S. Zhang, S. Wang, H. Tang, Efficient degradation of carbamazepine by easily recyclable micros-caled $CuFeO_2$ mediated heterogeneous activation of peroxy-monosulfate, J. Hazard. Mater., 317 (2016) 686–694.
[51] C. Liang, H.-W. Su, Identification of sulfate and hydroxyl radicals in thermally activated persulfate, Ind. Eng. Chem. Res., 48 (2009) 5558–5562.
[52] M. Usman, P. Faure, C. Ruby, K. Hanna, Application of magnetite-activated persulfate oxidation for the degradation of PAHs in contaminated soils, Chemosphere, 87 (2012) 234–240.
[53] K.-Y.A. Lin, Z.-Y. Zhang, Degradation of Bisphenol A using peroxymonosulfate activated by one-step prepared sulfur-doped carbon nitride as a metal-free heterogeneous catalyst, Chem. Eng. J., 313 (2017) 1320–1327.
[54] B. Darsinou, Z. Frontistis, M. Antonopoulou, I. Konstantinou, D. Mantzavinos, Sono-activated persulfate oxidation of bisphenol A: kinetics, pathways and the controversial role of temperature, Chem. Eng. J., 280 (2015) 623–633.
[55] H. Lin, J. Wu, H. Zhang, Degradation of clofibric acid in aqueous solution by an EC/Fe^{3+}/PMS process, Chem. Eng. J., 244 (2014) 514–521.
[56] Q. Yang, H. Choi, S.R. Al-Abed, D.D. Dionysiou, Iron–cobalt mixed oxide nanocatalysts: heterogeneous peroxymonosulfate activation, cobalt leaching, and ferromagnetic properties for environmental applications, Appl. Catal., B, 88 (2009) 462–469.
[57] X. Wang, L. Wang, J. Li, J. Qiu, C. Cai, H. Zhang, Degradation of Acid Orange 7 by persulfate activated with zero valent iron in the presence of ultrasonic irradiation, Sep. Purif. Technol., 122 (2014) 41–46.
[58] F. Ji, C. Li, L. Deng, Performance of CuO/oxone system: heterogeneous catalytic oxidation of phenol at ambient conditions, Chem. Eng. J., 178 (2011) 239–243.
[59] Q. Wang, X. Lu, Y. Cao, J. Ma, J. Jiang, X. Bai, T. Hu, Degradation of bisphenol S by heat activated persulfate: kinetics study, transformation pathways and influences of co-existing chemicals, Chem. Eng. J., 328 (2017) 236–245.
[60] J. Sharma, I.M. Mishra, D.D. Dionysiou, V. Kumar, Oxidative removal of Bisphenol A by UV-C/peroxymonosulfate (PMS): kinetics, influence of co-existing chemicals and degradation pathway, Chem. Eng. J., 276 (2015) 193–204.
[61] G.P. Anipsitakis, D.D. Dionysiou, Radical generation by the interaction of transition metals with common oxidants, Environ. Sci. Technol., 38 (2004) 3705–3712.
[62] J. García-Montaño, F. Torrades, J.A. García-Hortal, X. Domenech, J. Peral, Combining photo-Fenton process with aerobic sequencing batch reactor for commercial hetero-bireactive dye removal, Appl. Catal., B, 67 (2006) 86–92.